ARTICLE IN PRESS

Materials Science & Engineering A xxx (xxxx) xxx

ELSEVIER

Contents lists available at ScienceDirect

Materials Science & Engineering A

journal homepage: http://www.elsevier.com/locate/msea



High temperature nanoindentation of Cu-TiN nanolaminates

Jeffrey M. Wheeler ^{a,b}, Cayla Harvey ^c, Nan Li ^d, Amit Misra ^e, Nathan A. Mara ^f, Xavier Maeder ^b, Johann Michler ^b, Siddhartha Pathak ^{c,g,*}

- ^a ETH Zurich, Laboratory for Nanometallurgy, Department of Materials, Vladimir-Prelog-Weg 5, CH-8093 Zurich, Switzerland
- b Laboratory for Mechanics of Materials and Nanostructures, Empa, Swiss Federal Laboratories for Materials Science and Technology, Feuerwerkerstrasse 39, CH-3602, Thun, Switzerland
- ^c Chemical and Materials Engineering, University of Nevada, Reno, NV, 89557, USA
- d Center for Integrated Nanotechnologies, Los Alamos National Laboratory, Los Alamos, NM, 87545, USA
- ^e Materials Science and Engineering, University of Michigan, Ann Arbor, MI, 48109, USA
- f Department of Chemical Engineering and Materials Science, University of Minnesota, Minneapolis, MN 55455, USA
- ^g Department of Materials Science and Engineering, Iowa State University, Ames, IA, 50011, USA

ARTICLE INFO

Keywords: Indentation Nanolaminates Multilayers High temperature deformation Activation energy

ABSTRACT

We examined the high temperature indentation response of physical vapor deposited Cu–TiN multilayered nanocomposites with layer thicknesses ranging from 5 nm to 200 nm. A decrease in hardness with increasing temperature was observed, along with a strong correlation between the hardness and the nanometer-level TiN grain sizes, rather than layer thickness. The apparent activation energies calculated from the high temperature indentation experiments indicated that, for all but the smallest layer thicknesses, the deformation of copper in the nanolaminates dominate the plastic response in these composites. In the finest layer thicknesses, a decrease in the apparent activation energy value indicated possible co-deformation of Cu and TiN.

1. Introduction

Laminates composed of two or more phases with repeated nanoscale layer spacings have demonstrated enhanced mechanical properties due to strengthening mechanisms that incorporate the interaction of defects with bimetal interfaces, as well as dislocation confinement within a given phase [1,2]. In particular, metal/ceramic multilayered nanocomposites have attracted great interest due to their promising mechanical, chemical and physical properties, allowing them to be used in applications requiring a wide range of mechanical loads, temperatures, and other environmental conditions [3–10]. The combination of higher strength, high work hardening and formability of these metal/ceramic nanolaminates arises from the variation in strength and ductility between their constituent brittle (hard) ceramic and tough (soft) metal phases. However, the behavior of such nanolaminates as a function of temperature remains largely unknown, since only a few multilayered systems, and even fewer metal/ceramic systems, have been characterized at elevated temperatures so far [7,11,12].

Previous reports on nanolaminates under ambient conditions have investigated their mechanical properties and deformation behavior with

respect to changing layer thicknesses, observing high hardness and plastic co-deformation when the bi-layer thickness was reduced to nanometer levels [13]. Further investigations using high-resolution transmission electron microscopy and *in-situ* indentation have revealed dislocation activity in Al–TiN metal-ceramic multilayers [14]. Plastic co-deformation mechanisms were postulated for the improved ductility measured in these nanolayered metal/ceramics composite systems [13]. Additionally, atomic-scale modeling showed unit processes of single to a few dislocations operating during deformation at the metal/ceramic interfaces of NbC/Nb multilayers under different loading conditions of nanoindentation and uniaxial compression [15,16]. The peak flow strength and strain hardening of NbC/Nb multilayers were found to be associated with the slip transmission from Nb to NbC, and were correlated to the NbC layer thickness, the Nb layer thickness, and the interfacial dislocations.

Most reports in literature on metal-ceramic nanocomposites have examined layered structures with high aspect-ratio grains. For example, the in-plane grain size within layers were 2–10 times the individual layer thickness for metal/ceramics multilayers of Al–TiN synthesized using physical vapor deposition (PVD) [14,17,18]. In contrast, density

https://doi.org/10.1016/j.msea.2020.140522

Received 14 April 2020; Received in revised form 14 September 2020; Accepted 30 October 2020 Available online 13 November 2020 0921-5093/© 2020 Elsevier B.V. All rights reserved.

^{*} Corresponding author. 2220BP Hoover Hall, 528 Bissell Rd, Department of Materials Science and Engineering, Iowa State University, Ames, IA, 50011, USA. *E-mail addresses*: jeff.wheeler@mat.ethz.ch (J.M. Wheeler), caylaharvey@nevada.unr.edu (C. Harvey), nanli@lanl.gov (N. Li), amitmis@umich.edu (A. Misra), mara@umn.edu (N.A. Mara), xavier.maeder@empa.ch (X. Maeder), johann.michler@empa.ch (J. Michler), pathak@iastate.edu (S. Pathak).

functional theory (DFT) studies have suggested that Al has a stronger chemical affinity to bond with TiN, when compared to Cu [19]. Therefore, Cu and TiN are expected to exhibit a tendency towards 3-D island growth during sputtering of the nanolaminate films [20,21]. This is expected to result in a nanometer-scale grain size that is possibly smaller than the Cu-TiN individual layer thickness in the nanocomposite. In this work, we deposited Cu-TiN multilayers of varying individual layer thicknesses ranging from 5 to 200 nm. These multilayered nanocomposites were found to consist of nano-grained Cu and TiN layers, where the grain sizes were comparable to smaller than the respective layer thickness. Previous indentation studies on these Cu-TiN films with layer thickness varying from 5 to 200 nm in ambient conditions have revealed that the hardness has a weak dependence on the layer thickness and a stronger correlation with the grain size [10]. The objective of this study is to assess the elevated temperature deformation behavior in Cu-TiN nanolaminates with varying layer thicknesses (but having nanometer grain sizes) tested in a temperature range of 25–200 °C.

Only a few studies have investigated the high temperature response of metal/metal [22,23] and metal/ceramic nanolaminates [6,7]. For Cu-TiN multilayers, micro-pillar compression with three different layer thicknesses of 5-10 nm, 50-100 nm and 700-1000 nm had revealed that under ambient conditions, yielding was controlled by the size-dependent strength of Cu grains and the failure was caused by the shearing of the columnar grains of TiN. However, at elevated temperatures of 200-400 °C, the stress-assisted diffusion of the Cu layers had led to the extrusion of the copper layers from the free surface of micro-pillars, which was responsible for the subsequent yielding of the nanocomposite [7]. In order to investigate material response under the constraints of a different stress state, we utilize indentation testing in this work, where the constraint of the nanoindentation geometry is expected to largely prevent such extrusion events. Additionally the higher throughput of indentation testing allows us to investigate a wider range of Cu-TiN bilayer thicknesses over narrower temperature increments. Hence in this work we investigate the high temperature mechanical behavior under indentation in six different layer thicknesses of Cu-TiN multilayered thin films, with individual layer thicknesses ranging from 5 to 200 nm (in addition of non-laminated Cu and TiN), and over five different thermal histories.

2. Methods and materials

Multilayers of alternating Cu and TiN layers with a volume fraction of Cu:TiN = 1:1 were deposited using direct current (dc) magnetron sputtering at room temperature on Si substrates, the Si substrates have a thin top layer of amorphous SiO2. The Cu layers were deposited at a base pressure of 2×10^{-8} Torr. Reactive sputtering of Ti in a gas mixture of Ar and N (Ar:N = 30:3 SCCM) was used to deposit the TiN layers using with a bias of 20 W RF on the substrate. Six different individual (targeted) layer thicknesses were deposited for Cu-TiN: 5-5 nm, 10-10 nm, 20-20 nm, 50-50 nm, 100-100 nm and 200-200 nm. All samples had a total film thickness of $\sim 5~\mu m$. TEM was used to measure the actual layer thicknesses and grain sizes for the as-deposited Cu (5 nm) – TiN (5 nm) and Cu (50 nm) - TiN (50 nm) samples, as well as for the annealed Cu (5 nm) - TiN (5 nm), Cu (50 nm) - TiN (50 nm) and Cu (200 nm) - TiN (200 nm) multilayers. The multilayers were evaluated using crosssectional TEM; the as-deposited films were mechanically polished down to 20–30 µm thickness, followed by diamond lapping film down to 1 μm, and then finished by ion-milling in a GatanTM PIPSÒ instrument at 3-5 kV. TEM studies were conducted in a Tecnai TF 30TM 300 kV TEM. The TEM images were used for grain size distributions, which were determined by grain diameters measurements parallel to the interface.

Additionally, TiN grain sizes within the Cu–TiN layered samples were determined using X-ray diffraction (XRD). The Scherrer method was used to determine the grain sizes (*D*) of TiN grains from the Bragg-Brentano theta-2theta diffractogram [24,25]: $D = \frac{K\lambda}{\beta \cos \beta}$ where λ and β

are the wavelength of X-ray and the full width at half maximum (FWHM), θ is Bragg's angle and K the constant of proportionality. D was calculated using the (111) peak for TiN, and a K value of 0.9, which corresponds to spherical crystallites [24]. This result provides an estimation of the lower bounds as a few other factors, such as the presence of twins, crystal defects and microstrains, can also contribute to peak broadening [24,26]. For validation, the XRD measurements using the Scherrer method were compared to the TEM results on the same layer thicknesses. Acquisition parameters remained the same to allow for an accurate comparison for all samples analyzed using XRD and TEM.

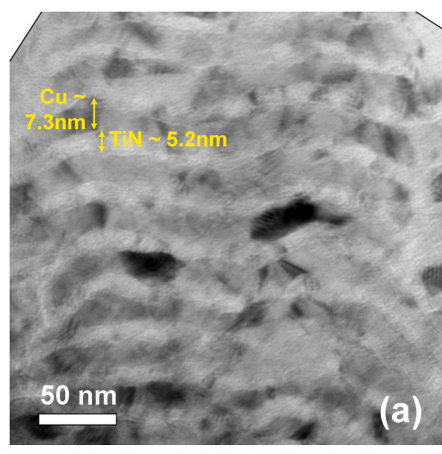
In situ, elevated temperature indentation testing [27] was conducted in a Zeiss DSM 962 SEM using an Alemnis in situ Indenter. The original system developed by Rabe et al. [28] was modified for elevated temperature testing through the incorporation of a water-cooled frame plus an independent sample and tip heating using thermocouple-controlled feedback loops along with the option of constant heating power at desired temperatures. Thermal drift was minimized at the testing temperatures by using both displacement drift [29] and temperature shift [30] tuning measurements during pseudo load-controlled indentation. Calibration of the indenter tip temperature was performed using the procedure described in Ref. [30,31]. The Alemnis system is intrinsically displacement-controlled, and tests were conducted to the target indentation depths described below after ensuring that the displacement and temperature drifts during contact were at their minimum.

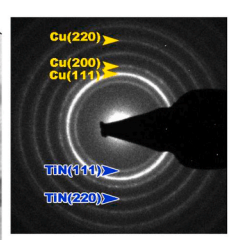
A diamond cube-corner indenter was used for the indentation experiments. Temperatures of 25, 90, 140, and 200 $^{\circ}$ C were used for the indentation experiments. These temperatures were selected to be at even homologous temperature intervals below the previously studied region 200–400 $^{\circ}$ C, where prominent extrusion of the Cu layers was observed under micro-compression [7]. The samples were first briefly heated to 75 $^{\circ}$ C to cure the mounting cement, and then the first tests were conducted at room temperature (25 $^{\circ}$ C). Then the samples were annealed at 200 $^{\circ}$ C for 14 h, followed by indentations at 200, 140, 90 and then 25 $^{\circ}$ C to determine nanolaminate performance as a function of temperature.

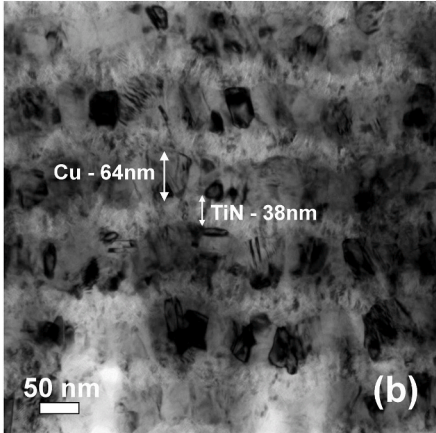
Standard constant loading rate indentations were made using the Oliver and Pharr method [32], with loading to maximum load performed within 10s, followed by a 10s hold period at maximum load. The indenter was then unloaded to 20% of the maximum load within 10s, then a 30s hold was applied to measure thermal drift levels, followed by removal of the indenter. The maximum loads were chosen for each material to reach a target maximum depth of $\sim 1 \mu m$: 3 mN for copper, 10 mN for the nanolaminates, and 30 mN for the TiN. These choices of indentation depth ensured that in each case the indenter was sampling regions within and beyond at least two bilayer thicknesses. As discussed later in the 'Results' section, this maximum indentation depth was also sufficiently larger than the grain sizes for both Cu and TiN. A minimum of 4 indentations were conducted in each condition. Our approach in this work is similar to the experimental design of our previous room temperature indentation study on the same range of Cu-TiN layer thicknesses [10], which allows these two studies to be comparable to each other.

3. Results

Characterization of the as deposited Cu–TiN multilayers highlights two major microstructural features: a wavy layered structure in the Cu–TiN films and a small grain size compared to the layer thickness. The TEM diffraction patterns and their corresponding micrographs of the as deposited Cu (5 nm) – TiN (5 nm) and Cu (50 nm) – TiN (50 nm) are shown in Fig. 1. Individual layer thicknesses for the Cu–TiN films with targeted thicknesses of 50-50 nm are measured to be $\sim\!64$ nm and $\sim\!38$ nm for Cu and TiN layers respectively, and the diffraction patterns indicate lack of a strong orientation relationship between the different layers. Fig. 2 shows the grain size distributions in the as-deposited Cu (5 nm) – TiN (5 nm) and Cu (50 nm) – TiN (50 nm) samples, as compared to the annealed Cu (5 nm) – TiN (5 nm), Cu (50 nm) – TiN (50 nm) and Cu







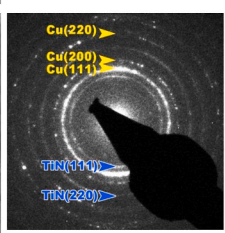


Fig. 1. Cross-sectional TEM with corresponding diffraction pattern of the as deposited (a) Cu (5 nm) – TiN (5 nm) (b) Cu (50 nm) – TiN (50 nm) layers.

(200 nm) - TiN (200 nm) samples.

For the as-deposited Cu-TiN film with targeted 5-5 nm thick layers (Figs. 1a and 2a), the actual layers were measured to be \sim 7.3 and \sim 5.2 nm for Cu and TiN layers respectively, the measured ring-shaped diffraction pattern is indicative of a lack of an orientation relationship with the TiN and Cu layers (Fig. 1a). This lack of a preferred texture is uniform amongst all the nanolaminates studied in this work, regardless of their bilayer thickness. Hence for comparative purposes, texture is considered to have only a tertiary effect on the indentation measurements (relative to bilayer thickness and temperature). The average grain sizes were measured to be 5.3 nm (range 2-8 nm) and 3.6 nm (range 2-5 nm) for Cu and TiN respectively (Fig. 2a). The average grain sizes for the as-deposited Cu (50 nm) - TiN (50 nm) sample were measured to be 24.5 nm (range 14-40 nm) and 4.4 nm (range 2-8 nm) for Cu and TiN respectively (Fig. 2b). These micrographs also reveal the waviness of the deposited layers, which is proposed to result from the dimensional island growth mechanism for Cu and TiN.

XRD measurements indicate that the TiN grain sizes are approximately independent of layer thickness. For all the multilayer samples, the as-deposited TiN grain sizes (1.5–4.5 nm range) were found to be smaller than the TiN layer thicknesses. Similarly, the as-deposited Cu grain sizes were also comparable to or smaller than the layer thickness for all layer thicknesses studied in this work [10].

After annealing, the grain sizes in both the TiN and Cu layers were found to increase for all layer thicknesses, as shown by the representative data for the Cu (5 nm) – TiN (5 nm), Cu (50 nm) – TiN (50 nm) and Cu (200 nm) – TiN (200 nm) samples in Fig. 2c–e. For the annealed Cu (5 nm) – TiN (5 nm) sample, the average grain size increased to $\sim\!10$ nm (range 2–22 nm) (Fig. 2c). For the larger layer thicknesses - Cu (50 nm) – TiN (50 nm) and Cu (200 nm) – TiN (200 nm) samples (Fig. 2d-e) – the

range of grain sizes in the TiN layers (range 4–9 nm) were still found to be smaller than the respective layer thickness, even after annealing. The range of grain sizes in the annealed Cu layers were larger (range 20–55 nm), but even for Cu the grain size was similar to or less than their respective layer thickness. TEM results indicated that the nanolaminate morphology was maintained after the annealing process, for all layer thicknesses.

The load-displacement results for the single component and nanolaminate coatings are shown in Fig. 3. In general, the total displacement was observed to increase with increasing temperature, indicating a decrease in hardness with temperature. Unloading stiffness values, and hence the elastic moduli, were observed to remain more or less constant with temperature within the experimental variation. This is unsurprising since only small changes are expected in the moduli of the Cu and TiN over the tested temperature range (129–120 GPa for Cu [33] and 466 to 460 GPa for TiN [34]).

Fig. 3a–d displays the load-displacement curves from the nanolaminate coatings. Some variation in the load is observed during the initial parts of the loading curves due to discrete inelastic events. In a typical, intrinsically load-controlled nanoindentation system, these would register as displacement bursts or pop-ins, however, in this pseudo-load controlled system the stresses are able to relax during inelastic events (such as plastic deformation or fracture) without generating additional displacements. This behavior is especially significant in the pure Cu sample in Fig. 3e, where a larger amount of variation is observed in the load signal during contact. The magnitude of these variations is higher than the noise floor of the instrument (5 μN RMS), so they can be attributed to the inelastic events. Fig. 3f shows that the TiN coating demonstrates largely athermal deformation at elevated temperatures.

Analysis of the load-displacement data using the Oliver and Pharr method [32] provides the hardness of the nanolaminate coatings over the range of temperatures tested in this work. This is shown in the hardness vs. bilayer thickness plot in Fig. 4a. Ambient temperature results (25 °C, after a brief 15 min curing of the mounting cement at 75 °C) display two separate regimes in hardness as a function of layer thickness. The Cu–TiN films with bilayer thicknesses of <40 nm show a small drop in hardness values (from 6.29 to 5.84 GPa), and the hardness values appear to saturate over the larger Cu-TiN bilayer thicknesses of 100, 200 and 400 nm with a slight decrease in hardness (5.24-5.39 GPa). The above trends at ambient temperatures are similar to those reported earlier in Ref. [10] using Berkovich indentations, where the weak dependence of hardness measurements on the layer thickness of Cu-TiN multilayers was attributed to the similar TiN grain sizes in these multilayers. Thus, the narrow hardness range observed in these Cu-TiN nanocomposites seems to stem from the small nanocrystalline TiN grain sizes, which range from 1.5 to 4.5 nm.

Hardness values were also measured after 14 h of annealing at 200 $^{\circ}$ C and cooling the samples down to room temperature. These hardnesses show a similar trend as described above, but with an overall decrease in the hardness values across all layer thicknesses, which can be attributed to the corresponding increase in TiN and Cu grain sizes after annealing (as shown in Fig. 2).

At elevated temperatures, we observe the expected decrease in hardness values across all layer thicknesses. Similar to the room temperature results, two distinct regimes of hardness values can be observed at the three elevated temperatures of 200, 140 and 90 $^{\circ}$ C as a function of changing layer thickness. At these temperatures, the Cu–TiN films with larger bilayer thicknesses of 400, 200, 100 and 40 nm show a lower range of hardness values (from 2.47 to 2.70 GPa at 200 $^{\circ}$ C, 2.79–3.06 GPa at 140 $^{\circ}$ C, and 3.35–3.63 GPa at 90 $^{\circ}$ C), as compared to the two lower bilayer thicknesses of 20 and 10 nm (from 3.38 to 3.73 GPa at 200 $^{\circ}$ C, 3.76–3.94 GPa at 140 $^{\circ}$ C, and 4.14–4.28 GPa at 90 $^{\circ}$ C).

As mentioned above, the determining factor of the strength in the Cu–TiN system is postulated to be the nano-crystalline grain sizes of the TiN layers. For the as-deposited Cu–TiN multilayers, the TiN grain sizes

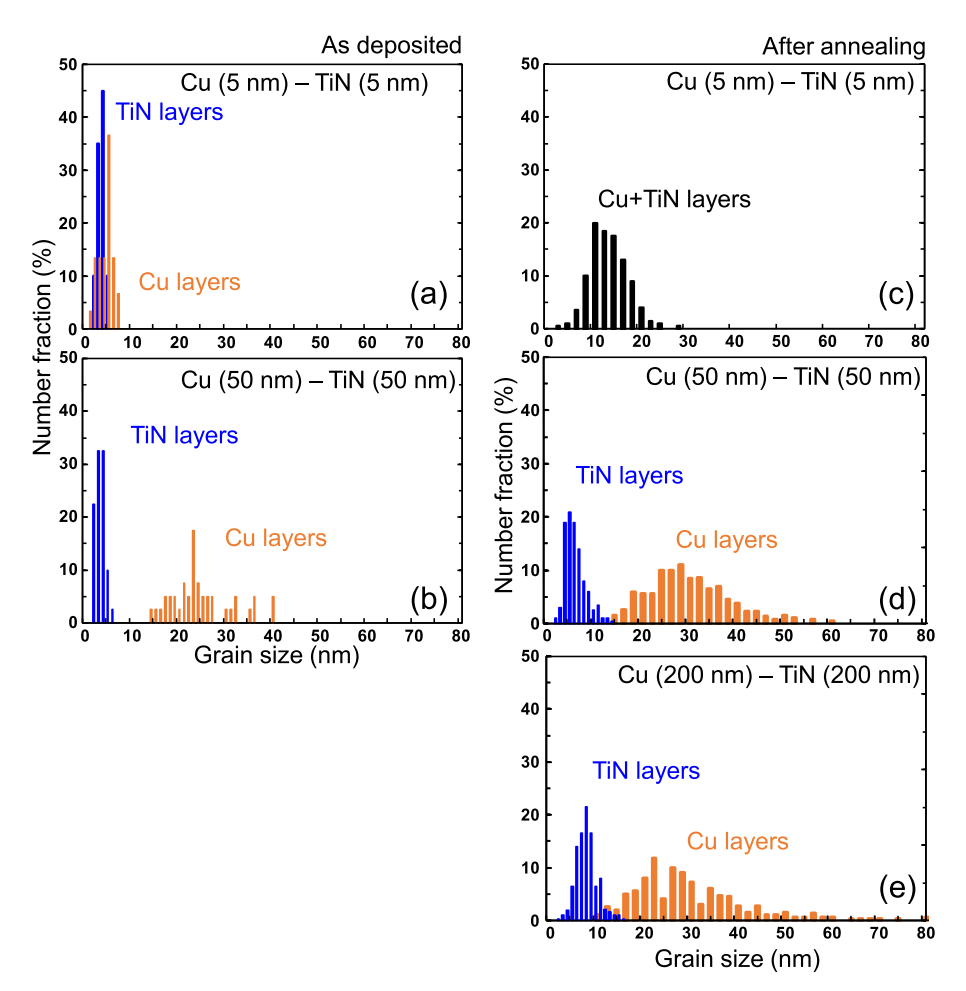


Fig. 2. Grain size distribution, measured using TEM, in the as deposited (a) Cu (5 nm) – TiN (5 nm), (b) Cu (50 nm) – TiN (50 nm) layers and the annealed (c) Cu (5 nm) – TiN (5 nm), (d) Cu (50 nm) – TiN (50 nm) and (e) Cu (200 nm) – TiN (200 nm) layers.

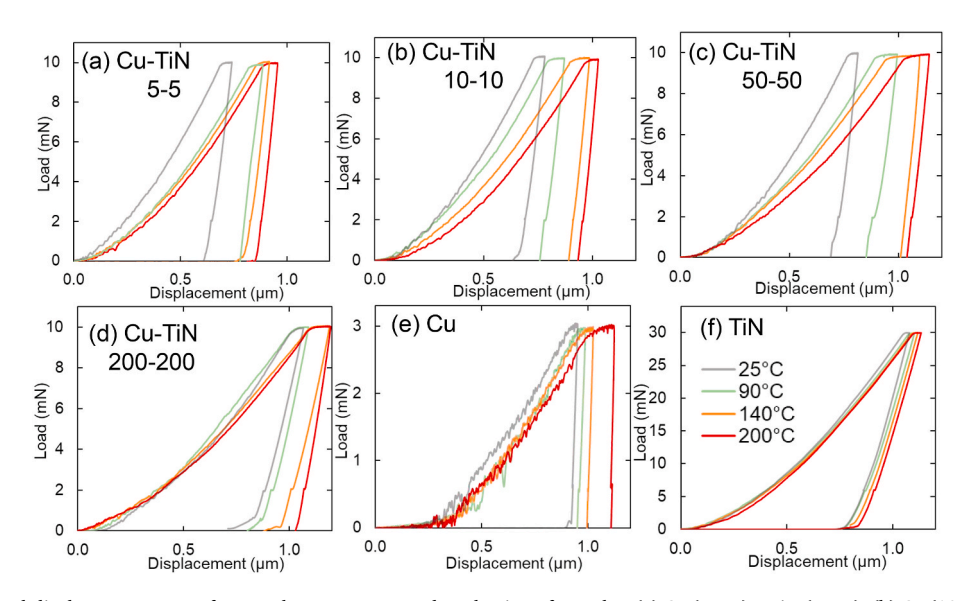


Fig. 3. Representative load-displacement curves from each temperature and a selection of samples: (a) Cu (5 nm) – TiN (5 nm), (b) Cu (10 nm) – TiN (10 nm), (c) Cu (50 nm) – TiN (50 nm), (d) Cu (200 nm) – TiN (200 nm), (e) Cu, and (f) TiN.

were measured to be in the range of 1.5–4.5 nm for all layer thicknesses [10]. After annealing, the TiN grain sizes were measured again using TEM for two selected layer thicknesses of Cu (50 nm) – TiN (50 nm) and Cu (200 nm) – TiN (200 nm). As shown in Figs. 2 and 4b, the average TiN

grain size for these two layer thicknesses ranged within 7.5–8 nm, which is slightly larger than the as deposited TiN grain sizes. Thus, the flat hardness regimes shown in Fig. 4a for the larger (>40 nm) bilayer thicknesses can be attributed to the near constant TiN grain size in these

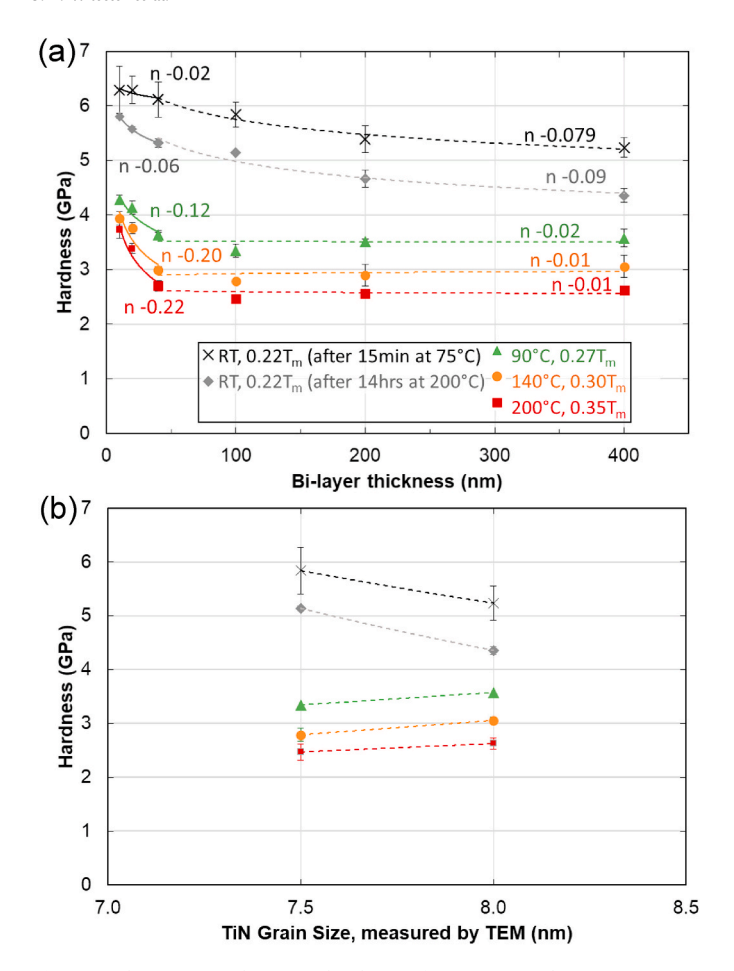


Fig. 4. Cube corner indentation hardness of Cu–TiN nanolaminate coatings under different temperature conditions: RT (25 °C), 90 °C, 140 °C, 200 °C, shown as a fraction of the homologous temperature (T_m) of Cu: a) vs bilayer thickness. The error bars denote the standard deviation of the hardness measurements. A power trend of $y = Ax^n$ was fit to the first three smallest bi-layer thickness and the last four largest layers, and the n coefficient is shown. b) Hardness vs. TiN grain size measured from TEM for the different bi-layer thickness laminates. TiN grain sizes are the smallest feature of interest in the largest layers.

layers. For the two smaller bilayer thicknesses of 20 and 10 nm, the TiN layer thickness is presumably smaller than or similar to the TiN grain sizes in these layers after annealing. Thus the hardness values in these layers show a stronger dependence on the layer thickness, i.e. the hardness increases with decreasing layer thickness.

The above observations are in contrast to other metal-ceramic multilayer systems, such as Al-TiN multilayers [17,18,35,36], where the smallest length scale of interest is the thickness of the individual layers which controls the hardness and strength in those systems (i.e. the individual layer thicknesses are smaller than the grain sizes in the Al-TiN multilayer structures). Also, co-deformation without cracking has been observed at individual layer thicknesses below ~5 nm in Al-TiN multilayers [17,18,35,36]. This enhanced co-deformability in nanoscale metal/ceramic nanolaminates is proposed to occur due to the high density of interfaces in 5 nm or smaller individual layer thicknesses of the Al-TiN system. At these dimensions, interactions between dislocations in the two adjacent interfaces are thought to produce high back stress in the metal layer (due to more pronounced strain hardening of the metal) and locally high resolved shear stress in ceramic nanolayers, enabling slip activity in the ceramic phase prior to fracture [13]. The smaller grain sizes in the Cu-TiN system, along with their lack of epitaxy, could potentially generate a larger density of interfaces in this multilayered system. This in turn could enable co-deformation and

enhanced plasticity in the Cu–TiN multilayered nanocomposites, especially for the lower layer thicknesses and grain sizes.

3.1. Discussion - apparent activation energy for deformation

Activation energy analysis allows the influence of thermal contributions on deformation to be quantified and compared to known values such as the activation energy for self-diffusion. As different materials possess varying temperature-dependence, this allows the primary deformation component to be determined in multicomponent systems like nanolaminates. Since deformation processes like dislocation glide and dislocation climb have greatly differing activation energies, this analysis can provide insight on which mechanisms are playing a role in deformation.

From the temperature-dependent hardness values acquired in the previous section, the apparent activation energy can be determined using an Arrhenius plot. Fig. 5 is a plot of the modulus-compensated hardness (H/E) with respect to the inverse homologous temperature. This removes the influence of modulus changes with changing temperatures from the activation analysis. The activation energy for plastic deformation can be calculated from the slope of these curves, following the analysis of Sherby & Armstrong [37,38]

$$\frac{H}{E} = G' \cdot \exp\left(\frac{Q_c}{nRT}\right)$$

where H is the hardness in GPa, E is the Young's modulus in GPa, G' is the pre-exponential coefficient, Q_c is the activation energy in kJ/mol, n is the stress exponent (assumed to be 5 for consistency with previous results [37,38]), R is the gas constant, and T is the absolute temperature in K. This analysis has been validated using hardness measurements at high homologous temperatures (>0.5 $T_{\rm m}$), where the resulting activation energy values corresponded well with self-diffusion values for pure bulk metals [37] and alloys [39], and more recently on the deformation of ultrafine-grained aluminum at lower homologous temperatures [40]. However, at low homologous temperatures the deformation might be athermal (i.e. the deformation might be independent of temperature and strain rate), and the activation energy values measured using this analysis could underestimate the true value. Hence we the use of the term 'apparent' activation energy, when referring to the values measured in this work. Furthermore, the measured 'apparent' activation energy values are used primarily to compare between the different layer thicknesses of the Cu-TiN multilayers, rather than as an absolute measurement.

The elastic modulus values used for normalizing the hardness in this analysis were taken to be the acoustically-measured values of the Young's modulus of copper from Köster [33], since the values for TiN were not expected to significantly change in this temperature range. Since the volume fractions of TiN and Cu were held nominally constant in all nanolaminates, the influence of the modulus change is expected to be uniform across all the samples.

Activation energy values are calculated only between the 90–200 °C temperature range, due to the significant variation observed in slope between 25 and 90 °C and the elevated temperature range. This low temperature regime was not well enough characterized to be able to clearly elucidate the operative deformation mechanisms. Fig. 5b shows the activation energy values calculated with respect to the bi-layer thickness in the Cu–TiN nanolaminates. The extracted activation energy values for the pure copper coatings (12 kJ/Mol) were found to be consistent with the results of Savitski (13 kJ/Mol) [41] for bulk copper indentation. For all but the two smallest bilayer thicknesses, the activation energy values were also found to be $\sim\!12$ kJ/Mol, which suggests that the deformation of the copper was the primary thermally activated mechanism in these coatings. In the finest layer thicknesses, the activation energy values were observed to significantly decrease, along with

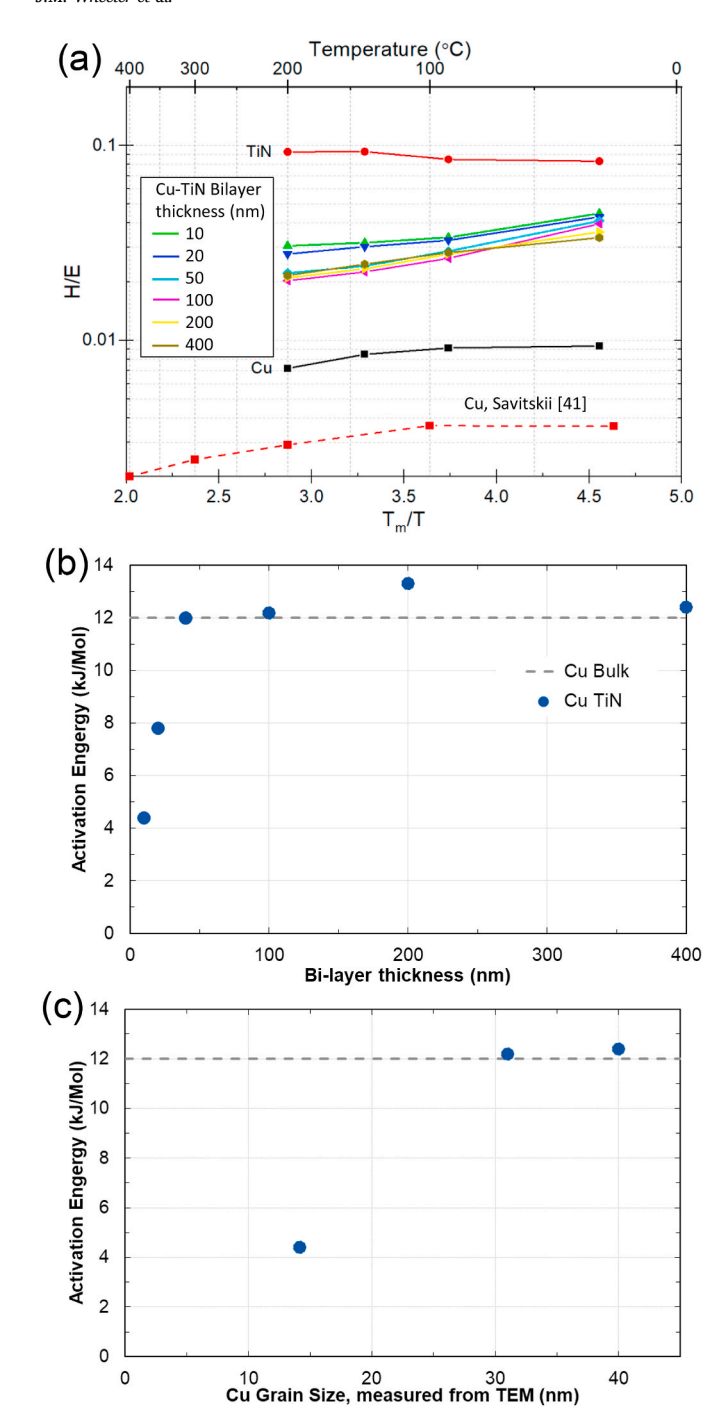


Fig. 5. (a) Modulus-compensated hardness as a function of the inverse homologous temperature for determining activation energies, showing results by Savitskii [41] on pure Cu and (b) measured activation energies from the 90–200 $^{\circ}$ C range vs. bilayer thickness and (c) vs. Cu grain size.

a decrease in the measured Cu grain sizes (Fig. 5c), suggesting that co-deformation of Cu and TiN may be occurring.

These results match those of other metal-ceramic multilayers, such as Al–SiC [6,42,43], where the ceramic component was shown to be effectively athermal, rigid and elastic as well. Micro-pillar compression of Al–SiC nanolaminates showed a larger increase in interface sliding with increasing temperature as well as homogenous plastic deformation was in the Al layers. Activation energies determined from indentation on these nanolaminates showed a SiC layers from 100 to 25 nm, with a constant 50 nm Al layer thickness, did not influence the activation energy. Similarly, the deformation of Cu–TiN at larger length scales

remains relatively constant.

4. Conclusions

In summary, our work investigated the behavior of Cu–TiN nanolaminate coatings using high temperature nanoindentation testing, revealing a decrease in hardness with temperature. These composites consisted of continuous layered structures, but with nanocrystalline grain sizes within the constituent layers. Hence, the hardness of these nano-composites were found to depend on the intra-layer grain sizes, with a relatively weaker dependence on the inter-layer spacing. Two separate regimes in hardness as a function of layer thickness were observed in these multilayers at all temperatures. Apparent activation energies estimated from the measured temperature dependence of hardness suggest that Cu dominated the plastic response at elevated temperatures for all coatings except those with the smallest bilayer thicknesses of $\approx\!10$ nm. For the smallest layers the activation energy values significantly decreased, suggesting a plastic co-deformation of nanolayered Cu and TiN.

CRediT authorship contribution statement

Jeffrey M. Wheeler: Conceptualization, Methodology, Investigation, Investigation, Writing - review & editing. Cayla Harvey: Writing - review & editing. Nan Li: Investigation. Amit Misra: Validation, writing. Nathan A. Mara: Validation, writing. Xavier Maeder: Supervision. Johann Michler: Supervision. Siddhartha Pathak: Conceptualization, Methodology, Investigation, Investigation, Writing - review & editing, Supervision.

Declaration of competing interest

The authors declare that they have no known competing financial interests or personal relationships that could have appeared to influence the work reported in this paper.

Acknowledgements

The authors would like to thank D. Frey & G. Buerki for technical assistance with the *In Situ* Indenter and S. Hostettler of Synton-MDP AG, Nidau, Switzerland for help with the joint development of the heated indenter tips used in this work. SP acknowledges equipment funding from NSF MRI #1726897 and DOE DE-NE0008739, and research funding from NSF CMMI #1841331 for this work.

Part of this research was sponsored by the US Army Research Office (ARO) and was accomplished under Grant Number: W911NF-19-1-0389. The views and conclusions contained in this document are those of the authors and should not be interpreted as representing the official policies, either expressed or implied, of ARO or the U.S. Government. The U.S. Government is authorized to reproduce and distribute reprints for Government purposes notwithstanding any copyright notation herein.

This work was performed, in part, at the Center for Integrated Nanotechnologies, an Office of Science User Facility operated for the U. S. Department of Energy (DOE) Office of Science. Los Alamos National Laboratory, an affirmative action equal opportunity employer, is managed by Triad National Security, LLC, for the National Nuclear Security Administration of the U.S. Department of Energy under contract 89233218CNA000001.

References

- M.J. Buehler, A. Misra, Mechanical behavior of nanocomposites, MRS Bull. 44 (1) (2019) 19–24.
- [2] I.J. Beyerlein, M.J. Demkowicz, A. Misra, B.P. Uberuaga, Defect-interface interactions, Prog. Mater. Sci. 74 (2015) 125–210.

- [3] I. Salehinia, S. Shao, J. Wang, H.M. Zbib, Plastic deformation of metal/ceramic nanolayered composites, J. Occup. Med. 66 (10) (2014) 2078–2085.
- [4] T.P.D. Rajan, B.C. Pai, Developments in processing of functionally gradient metals and metal-ceramic composites: a review, Acta Metallurgica Sinica-English Letters 27 (5) (2014) 825–838.
- [5] I. Knorr, N.M. Cordero, E.T. Lilleodden, C.A. Volkert, Mechanical behavior of nano scale Cu/PdSi multilayers, Acta Mater. 61 (13) (2013) 4984–4995.
- [6] S. Lotfian, J.M. Molina-Aldareguia, K.E. Yazzie, J. Llorca, N. Chawla, High-temperature nanoindentation behavior of Al/SiC multilayers, Phil. Mag. Lett. 92 (8) (2012) 362–367.
- [7] R. Raghavan, J.M. Wheeler, D. Esque-de los Ojos, K. Thomas, E. Almandoz, G. G. Fuentes, J. Michler, Mechanical behavior of Cu/TiN multilayers at ambient and elevated temperatures: stress-assisted diffusion of Cu, Materials Science and Engineering a-Structural Materials Properties Microstructure and Processing 620 (2015) 375–382.
- [8] I. Salehinia, S. Shao, J. Wang, H.M. Zbib, Interface structure and the inception of plasticity in Nb/NbC nanolayered composites, Acta Mater. 86 (2015) 331–340.
- [9] L.W. Yang, C. Mayer, N. Li, J.K. Baldwin, N.A. Mara, N. Chawla, J.M. Molina-Aldareguia, J. Llorca, Mechanical properties of metal-ceramic nanolaminates: effect of constraint and temperature, Acta Mater. 142 (2018) 37–48.
- [10] S. Pathak, N. Li, X. Maeder, R.G. Hoagland, J.K. Baldwin, J. Michler, A. Misra, J. Wang, N.A. Mara, On the origins of hardness of Cu–TiN nanolayered composites, Scripta Mater. 109 (2015) 48–51.
- [11] J.M. Wheeler, R. Raghavan, V. Chawla, J. Zechner, I. Utke, J. Michler, Failure mechanisms in metal—metal nanolaminates at elevated temperatures: microcompression of Cu–W multilayers, Scripta Mater. 98 (2015) 28–31.
- [12] R. Raghavan, J.M. Wheeler, T.P. Harzer, V. Chawla, S. Djaziri, K. Thomas, B. Philippi, C. Kirchlechner, B.N. Jaya, J. Wehrs, J. Michler, G. Dehm, Transition from shear to stress-assisted diffusion of copper-chromium nanolayered thin films at elevated temperatures, Acta Mater. 100 (2015) 73–80.
- [13] J. Wang, A. Misra, Strain hardening in nanolayered thin films, Curr. Opin. Solid State Mater. Sci. 18 (1) (2014) 19–28.
- [14] N. Li, H. Wang, A. Misra, J. Wang, In situ nanoindentation study of plastic Codeformation in Al-TiN nanocomposites, Sci. Rep. 4 (2014).
- [15] I. Salehinia, S. Shao, J. Wang, H.M. Zbib, Interface structure and the inception of plasticity in Nb/NbC nanolayered composites, Acta Mater. 86 (2015) 331–340.
- [16] I. Salehinia, J. Wang, D.F. Bahr, H.M. Zbib, Molecular dynamics simulations of plastic deformation in Nb/NbC multilayers, Int. J. Plast. 59 (2014) 119–132.
- [17] D. Bhattacharyya, N.A. Mara, P. Dickerson, R.G. Hoagland, A. Misra, Compressive flow behavior of Al-TiN multilayers at nanometer scale layer thickness, Acta Mater. 59 (10) (2011) 3804–3816.
- [18] D. Bhattacharyya, N.A. Mara, R.G. Hoagland, A. Misra, Nanoindentation and microstructural studies of Al/TiN multilayers with unequal volume fractions, Scripta Mater. 58 (11) (2008) 981–984.
- [19] S.K. Yadav, R. Ramprasad, J. Wang, A. Misra, X.Y. Liu, First-principles study of Cu/ TiN and Al/TiN interfaces: weak versus strong interfaces, Model. Simulat. Mater. Sci. Eng. 22 (3) (2014), 035020.
- [20] S.J. Liu, H. Huang, C.H. Woo, Schwoebel-Ehrlich barrier: from two to three dimensions, Appl. Phys. Lett. 80 (18) (2002) 3295–3297.
- [21] H. Huang, J. Wang, Surface kinetics: step-facet barriers, Appl. Phys. Lett. 83 (23) (2003) 4752–4754.
- [22] K. Thomas, G. Mohanty, J. Wehrs, A.A. Taylor, S. Pathak, D. Casari, J. Schwiedrzik, N. Mara, R. Spolenak, J. Michler, Elevated and cryogenic temperature micropillar compression of magnesium-niobium multilayer films, J. Mater. Sci. 54 (15) (2019) 10884–10901.
- [23] J.T. Avallone, T.J. Nizolek, B.B. Bales, T.M. Pollock, Creep resistance of bulk copper–niobium composites: an inverse effect of multilayer length scale, Acta Mater. 176 (2019) 189–198.

- [24] J.I. Langford, A.J.C. Wilson, Scherrer after sixty years: a survey and some new results in the determination of crystallite size, J. Appl. Crystallogr. 11 (2) (1978) 102–113.
- [25] A.L. Patterson, The scherrer formula for X-ray particle size determination, Phys. Rev. 56 (10) (1939) 978–982.
- [26] Z. Zhang, F. Zhou, E.J. Lavernia, On the analysis of grain size in bulk nanocrystalline materials via x-ray diffraction, Metall. Mater. Trans. 34 (6) (2003) 1349–1355.
- [27] J.M. Wheeler, J. Michler, Elevated temperature, nano-mechanical testing in situ in the scanning electron microscope, Rev. Sci. Instrum. 84 (4) (2013), 064303.
- [28] R. Rabe, J.M. Breguet, P. Schwaller, S. Stauss, F.J. Haug, J. Patscheider, J. Michler, Observation of fracture and plastic deformation during indentation and scratching inside the scanning electron microscope, Thin Solid Films 469–470 (2004) 206–213.
- [29] S. Korte, W.J. Clegg, Micropillar compression of ceramics at elevated temperatures, Scripta Mater. 60 (9) (2009) 807–810.
- [30] J.M. Wheeler, P. Brodard, J. Michler, Elevated temperature, in situ indentation with calibrated contact temperatures, Philos. Mag. A 92 (25–27) (2012) 3128–3141
- [31] J.M. Wheeler, R. Raghavan, J. Michler, In situ SEM indentation of a Zr-based bulk metallic glass at elevated temperatures, Mater. Sci. Eng. 528 (29–30) (2011) 8750–8756.
- [32] W.C. Oliver, G.M. Pharr, An improved technique for determining hardness and elastic-modulus using load and displacement sensing indentation experiments, J. Mater. Res. 7 (6) (1992) 1564–1583.
- [33] W. Koster, Die temperaturabhangigkeit des elastizitatsmoduls reiner metalle, Zeitschrift fur Metallkunde 39 (1) (1948) 1–9.
- [34] P. Steneteg, O. Hellman, O.Y. Vekilova, N. Shulumba, F. Tasnádi, I.A. Abrikosov, Temperature dependence of TiN elastic constants from ab initio molecular dynamics simulations, Phys. Rev. B 87 (9) (2013), 094114.
- [35] D. Bhattacharyya, N.A. Mara, P. Dickerson, R.G. Hoagland, A. Misra, Transmission electron microscopy study of the deformation behavior of Cu/Nb and Cu/Ni nanoscale multilayers during nanoindentation, J. Mater. Res. 24 (3) (2009) 1291–1302.
- [36] D. Bhattacharyya, N.A. Mara, P. Dickerson, R.G. Hoagland, A. Misra, A transmission electron microscopy study of the deformation behavior underneath nanoindents in nanoscale Al-TiN multilayered composites, Phil. Mag. 90 (13) (2010) 1711–1724.
- [37] O.D. Sherby, P.E. Armstrong, Prediction of activation energies for creep and self-diffusion from hot hardness data. Metall. Mater. Trans. B 2 (12) (1971) 3479–3484.
- [38] O.D. Sherby, P.M. Burke, Mechanical behavior of crystalline solids at elevated temperature, Prog. Mater. Sci. 13 (1968) 323–390.
- [39] G.S. Sohal, R. Pearce, Activation energies for the deformation of superplastic alloys and their phases derived from hot microhardness studies, J. Mater. Sci. 22 (7) (1987) 2327–2331.
- [40] J.M. Wheeler, V. Maier, K. Durst, M. Göken, J. Michler, Activation parameters for deformation of ultrafine-grained aluminium as determined by indentation strain rate jumps at elevated temperature, Mater. Sci. Eng. 585 (2013) 108–113.
- [41] E.M.E.M. Savitskii, The Influence of Temperature on the Mechanical Properties of Metals and Alloys, Stanford University Press1961.
- [42] S. Lotfian, C. Mayer, N. Chawla, J. Llorca, A. Misra, J.K. Baldwin, J.M. Molina-Aldareguía, Effect of layer thickness on the high temperature mechanical properties of Al/SiC nanolaminates, Thin Solid Films 571 (2) (2014) 260–267.
- [43] S. Lotfian, M. Rodríguez, K.E. Yazzie, N. Chawla, J. Llorca, J.M. Molina-Aldareguía, High temperature micropillar compression of Al/SiC nanolaminates, Acta Mater. 61 (12) (2013) 4439–4451.